Biochimica et Biophysica Acta 1818 (2012) 318–329

Contents lists available at SciVerse ScienceDirect

Biochimica et Biophysica Acta

journal homepage: www.elsevier.com/locate/bbamem

Review

Charge equilibration force fields for molecular dynamics simulations of lipids, bilayers, and integral membrane protein systems ☆

Timothy R. Lucas, Brad A. Bauer, Sandeep Patel *

Department of Chemistry and Biochemistry, University of Delaware, Newark, Delaware 19716, USA

ARTICLE INFO

Article history:
Received 3 July 2011
Received in revised form 13 September 2011
Accepted 14 September 2011
Available online 24 September 2011

Keywords:
Charge equilibration
Polarizable force field
Molecular dynamics simulation
Lipid
Bilayer

ABSTRACT

With the continuing advances in computational hardware and novel force fields constructed using quantum mechanics, the outlook for non-additive force fields is promising. Our work in the past several years has demonstrated the utility of polarizable force fields, those based on the charge equilibration formalism, for a broad range of physical and biophysical systems. We have constructed and applied polarizable force fields for lipids and lipid bilayers. In this review of our recent work, we discuss the formalism we have adopted for implementing the charge equilibration (CHEQ) method for lipid molecules. We discuss the methodology, related issues, and briefly discuss results from recent applications of such force fields. Application areas include DPPC-water monolayers, potassium ion permeation free energetics in the gramicidin A bacterial channel, and free energetics of permeation of charged amino acid analogs across the water-bilayer interface. This article is part of a Special Issue entitled: Membrane protein structure and function.

Contents

1. Introduction

Computational chemistry is an indispensable tool in the arsenal of today's chemist, biochemist, and biologist. It is thus not surprising that the computational modeling community continues to push for advanced methods and models at a feverish pace. The advances have become ever faster in the recent decades due to the increased computational resources emerging as high-performance computer hardware becomes available to the masses at commodity prices. Along with the advances in hardware and software, algorithmic and force field developments have impacted the state-of-the-art profoundly. Though the issues of sampling on accurate (free) energy surfaces are intimately coupled to the force field and capabilities of

☆ This article is part of a Special Issue entitled: Membrane protein structure and function.

* Corresponding author.
E-mail address: sapatel@udel.edu (S. Patel).

0005-2736/$ – see front matter © 2011 Published by Elsevier B.V.
doi:10.1016/j.bbamem.2011.09.016

available hardware, work continues on both fronts along fairly independent lines, largely due to the fact that both problems are profoundly difficult to tackle simultaneously with current resources. This review article deals with the aspect of molecular interaction models, and in particular, models based on non-additive electrostatic interactions. For the purposes of this review, we consider non-additive electrostatic models as those which allow for the variation of the local molecular electrostatic environment (i.e., charges, dipole moments, higher-order electrostatic moments) based on some predefined, systematic theoretical formalism. Work in the recent decades has realized the need to revisit the implications of electrostatic polarizability in defining the quality of molecular simulations [1–17]. As a result, the development of models that explicitly treat polarizability has been steadily progressing. Considering the formalisms for modeling molecular polarizability in a classical treatment, point-dipole (and higher-order multipole) [7,8,18–25], Drude oscillator [26–35], ab initio-inspired methods [17,36–41], and charge equilibration/fluctuating charge [3,5,6,42–55] models are currently being developed. A detailed comparison among these approaches is beyond the scope of the current work, however, Illingworth and Domene have addressed such comparisons in a recent review [56]. The charge equilibration approach, which is used extensively by our group, is discussed in detail in the next section.

In general, polarization methods consider the induction of a dipole moment (μ_{ind}) in the presence of an electric field ($\mathbf{E}$):

$$\mu_{ind} = \alpha \mathbf{E}. \tag{1}$$

These formalisms differ in the treatment of the polarizability, α.

Though there are rational arguments indicating that the molecular polarizability in the condensed phase might be somewhat reduced compared to gas phase, there is no clear absolute estimate of this reduction due to the difficulty associated with unambiguously computing this property in the condensed phase. Thus, α is adjusted empirically. The nature of the condensed phase polarizability can be treated in an ad hoc manner via scaling to reproduce certain target properties of condensed phase and gas-phase cluster models. In other cases, the gas-phase polarizability is applied directly for models of the condensed phase; the parameters of the model then implicitly account for the variation of polarizability with environment (condensed phase versus gas-phase) [7,8,23,57,58].

The application of polarizable force fields, or at least models that allow for the molecular response of system components to changes in local electrochemical environment, appears to be a natural tool for adding further physical elements to the modeling of highly anisotropic environments such as bilayers. For example, the dramatic change in dielectric constant progressing from the bulk solution (aqueous environment with static dielectric constant in the vicinity of 78) to the bilayer interior (almost vacuum-like environment for a single solute, with dielectric constant of approximately 2) suggests that molecular properties such as molecular dipole moments for polar species can drastically change. Such a simple, perhaps nuanced, physical effect can have profound effects on a wide variety of phenomena. Thus, we seek to develop models capable of treating such electrostatic effects at the most basic level in order to ultimately glean novel mechanistic and/or energetic insights.

In the following, we discuss our development methodology, and then recent applications of the force fields for molecular dynamics studies involving bilayer systems.

2. Force fields

2.1. Charge equilibration force fields

We next consider details of the charge equilibration (CHEQ) method and considerations in our specific implementation of this method. An additive (or *non-polarizable*) formalism for force fields is based on the construct that all atomic partial charges are fixed throughout the course of the simulations. Alternatively, we can consider the variation of atomic partial charge using the CHEQ formalism [3,5,6,42–48,50]. The CHEQ formalism is based on Sanderson's idea of electronegativity equilibration [42,43] in which the chemical potential is equilibrated via the redistribution of charge density. In a classical sense, charge density is reduced to partial charges, Q_α on each atomic site α. The charge-dependent energy for a system of M molecules containing N_i atoms per molecule is then expressed as

$$E_{CHEQ}\left(\vec{R},\vec{Q}\right) = \sum_{i=1}^{M}\sum_{\alpha=1}^{N}\chi_{i\alpha}Q_{i\alpha} + \frac{1}{2}\sum_{i=1}^{M}\sum_{j=1}^{M}\sum_{\alpha=1}^{N_i}\sum_{\beta=1}^{N_j}J_{i\alpha j\beta}Q_{i\alpha}Q_{j\beta} + \frac{1}{2}\sum_{i=1}^{MN}{}'\sum_{j=1}^{MN}{}'\frac{Q_iQ_j}{4\pi\epsilon_0 r_{ij}} + \sum_{j=1}^{M}\lambda_j\left(\sum_{i=1}^{N}Q_{ji} - Q_j^{Total}\right) \tag{2}$$

where the χ terms represent the atomic electronegativities which control the directionality of electron flow and J terms represent the atomic hardnesses which control the resistance to electron flow to or from the atom. Although these parameters are derived from the definitions of electron affinity and ionization potential, they are treated as empirical parameters for individual atom types. Heterogeneous hardness elements that describe the interaction between two different atom types are calculated using the combining rule [59] on the parameterized homogeneous hardness elements (J_{ii}°):

$$J_{ij}\left(R_{ij},J_{ii}^{\circ},J_{jj}^{\circ}\right) = \frac{\frac{1}{2}\left(J_{ii}^{\circ}+J_{jj}^{\circ}\right)}{\sqrt{1.0+\frac{1}{4}\left(J_{ii}^{\circ}+J_{jj}^{\circ}\right)^2 R_{ij}^2}} \tag{3}$$

where R_{ij} is the distance between atoms i and j. This combination locally screens Coulombic interactions, but provides the correct limiting behavior at atomic separations greater than approximately 2.5 Å. The standard Coulomb interaction between sites not involved in the dihedral, angle, or bonded interactions (denoted by primed summation) with each other is included as the third term in Eq. (2). The second term in Eq. (2) represents the local charge transfer interaction, which is usually restricted to within a molecule or an appropriate charge normalization unit. Currently, we do not consider intermolecular charge transfer, although approaches to incorporate this effect have recently been developed and applied to liquid water [60]. Charge is constrained via a Lagrange multiplier, λ, which is included for each molecule as indicated in the last term of Eq. (2). We remark that use of multiple charge normalization units can modulate molecular polarizability by limiting intramolecular charge transfer to physical distances. Such an approach controls previously observed superlinear polarizability scaling [52,54,61], which also manifests as the polarization catastrophe (in point polarizable force fields) [8,52], while also developing a construct for piecing together small molecular entities into macromolecules.

Charge degrees of freedom are propagated via an extended Lagrangian formulation, thus providing for electronegativity equilibration at each dynamics step. The system Lagrangian is:

$$L = \sum_{i=1}^{M}\sum_{\alpha=1}^{N}\frac{1}{2}m_{i\alpha}\left(\frac{dr_{i\alpha}}{dt}\right)^2 + \sum_{i=1}^{M}\sum_{\alpha=1}^{N}\frac{1}{2}m_{Q,i\alpha}\left(\frac{dQ_{i\alpha}}{dt}\right)^2 - E(Q,r) - \sum_{i=1}^{M}\lambda_i\sum_{\alpha=1}^{N}Q_{i\alpha} \tag{4}$$

where the first two terms represent the nuclear and charge kinetic energies, the third term is the potential energy, and the fourth term is the molecular charge neutrality constraint enforced on each

molecule i via a Lagrange multiplier λ_i. The fictitious charge dynamics are determined using a charge "mass" with units of (energy time^2/charge^2), which is analogous to the use of an adiabaticity parameter in fictitious wavefunction dynamics in Car Parinello (CP) type methods [3,62]. Charges are propagated based on the forces arising from differences between the average electronegativity of a molecule and the instantaneous electronegativity at an atomic site.

2.2. Polarizability in charge equilibration models

When the electrostatic energy expression for a single molecule comprised of N atoms is differentiated with respect to charge and set equal to zero, a set of N equations can be solved to determine the set of charges which minimizes the energy. This set of equations can be recast in matrix form as

$$\mathbf{JQ} = -\chi \tag{5}$$

where $\mathbf{J}$ is the atomic hardness matrix, $\mathbf{Q}$ is the atomic charge vector, and χ is the atomic electronegativity vector. Written explicitly, the matrix representation is:

$$\begin{bmatrix} J_{11} & J_{12} & \cdots & \cdots & J_{1N} \\ J_{21} & \ddots & & & \vdots \\ \vdots & & \ddots & & \vdots \\ \vdots & & & \ddots & \vdots \\ J_{N1} & \cdots & \cdots & \cdots & J_{NN} \end{bmatrix} \begin{bmatrix} Q_1 \\ Q_2 \\ \vdots \\ \vdots \\ Q_N \end{bmatrix} = - \begin{bmatrix} \chi_1 \\ \chi_2 \\ \vdots \\ \vdots \\ \chi_N \end{bmatrix}. \tag{6}$$

These equations can be augmented to include the charge conservation constraint that the sum of atomic charges must equal the net charge on the molecule,

$$\sum_{i=1}^{M} Q_i = Q_{net}. \tag{7}$$

The inclusion of this additional constraint produces a modified set of equations:

$$\mathbf{J}'Q' = -\chi'; \tag{8}$$

which is written explicitly as:

$$\begin{bmatrix} J_{11} & J_{12} & \cdots & \cdots & J_{1N} & 1 \\ J_{21} & \ddots & & & \vdots & 1 \\ \vdots & & \ddots & & \vdots & \vdots \\ \vdots & & & \ddots & \vdots & \vdots \\ J_{N1} & \cdots & \cdots & \cdots & J_{NN} & 1 \\ 1 & \cdots & \cdots & \cdots & 1 & 0 \end{bmatrix} \begin{bmatrix} Q_1 \\ Q_2 \\ \vdots \\ \vdots \\ Q_N \\ \lambda \end{bmatrix} = - \begin{bmatrix} \chi_1 \\ \chi_2 \\ \vdots \\ \vdots \\ \chi_N \\ Q_{net} \end{bmatrix}. \tag{9}$$

As alluded to in the previous section, it is appropriate to limit the extent of intramolecular charge transfer by introducing additional charge constraints. Such a consideration is particularly important in large biological systems. In practice, the total charge of the molecule is constrained to Q_{net} while additionally enforcing the requirement that the sum of charges for a subset of atoms within the molecule to equal a specified quantity, $Q_{net,k}$. We refer to this subset of atoms as a charge conservation unit. Since the net charge over the entire molecule must be maintained, the following condition must hold:

$$Q_{net} = \sum_{k=1}^{M} Q_{net,k}, \tag{10}$$

in which M denotes the number of charge conservation units. We can extend our previous illustration of the system of equations generated with a single charge constraint (Eq. 9) to show the set of equations when a molecule is broken into two charge conservation units:

$$\begin{bmatrix} J_{11} & \cdots & J_{1h} & J_{1(h+1)} & \cdots & J_{1N} & 1 & 0 \\ \vdots & \ddots & & & & \vdots & \vdots & \vdots \\ J_{h1} & & J_{hh} & & & \vdots & 1 & 0 \\ J_{(h+1)1} & & & J_{(h+1)(h+1)} & & \vdots & 0 & 1 \\ \vdots & & & & \ddots & \vdots & \vdots & \vdots \\ J_{N1} & \cdots & J_{Nh} & J_{N(h+1)} & \cdots & J_{NN} & 0 & 1 \\ 1 & \cdots & 1 & 0 & \cdots & 0 & 0 & 0 \\ 0 & \cdots & 0 & 1 & \cdots & 1 & 0 & 0 \end{bmatrix} \begin{bmatrix} Q_1 \\ \vdots \\ Q_h \\ Q_{h+1} \\ \vdots \\ Q_N \\ \lambda_1 \\ \lambda_2 \end{bmatrix} = - \begin{bmatrix} \chi_1 \\ \vdots \\ \chi_h \\ \chi_{h+1} \\ \vdots \\ \chi_N \\ Q_{net,1} \\ Q_{net,2} \end{bmatrix}. \tag{11}$$

For this example, atomic sites 1 through h are grouped into one charge conservation unit, while atomic sites $h+1$ through N are grouped into a second charge normalization unit. In the augmented atomic hardness matrix, values of 1 in element $(i,N+1)$ or $(N+1,i)$ denote that atom i is assigned to the first charge conservation unit (which has a net charge of $Q_{net,1}$). Similarly, values of 1 in elements $(i,N+2)$ or $(N+2,i)$ denote that atom i is assigned to the second charge conservation unit (with net charge $Q_{net,2}$).

The molecular polarizability in the CHEQ formalism can be calculated as [52]:

$$\alpha_{\gamma\beta} = \mathbf{R}_\beta^T \mathbf{J}'^{-1} \mathbf{R}_\gamma \tag{12}$$

where $\mathbf{J}'$ is the atomic hardness matrix augmented with the appropriate rows and columns to treat the charge conservation constraints. $\mathbf{R}_\gamma$ and $\mathbf{R}_\beta$ are the γ and β Cartesian coordinates of the atomic position vectors; these vectors are augmented to appropriately match the dimensions of the atomic hardness matrix. Representative values for the molecular polarizability are given in Ref. [47].

3. Development of CHEQ lipid bilayer force fields

Membranes and membrane-bound proteins are a vital part of biological systems. Recent studies have explored structural properties of membranes and electrostatic properties such as the dielectric variation within a bilayer, [63] the interfacial potential, [64] and the interactions of polar or charged amino acid side chains with hydrocarbon tails [65]. Experimental studies have also probed these properties in recent years. For example, structural properties of bilayers have been determined by X-ray and neutron scattering [66,67] and nuclear magnetic resonance (NMR) spectroscopy, [68] while the water penetration into the bilayer interior has been investigated via electron spin spectroscopy [69,70] and X-ray scattering techniques [71]. However, even current state-of-the-art experimental measurements are not always able to provide the type of detailed atomic level resolution that would provide significant insights into the mechanisms involving membrane systems. To this end, computational methods such as molecular dynamics and Monte Carlo simulations have been employed to study properties and processes in such systems at the atomic level [65,72–86].

Recently, we have developed non-additive, charge equilibration (CHEQ) force fields for lipid bilayers based on dimirystoylphosphatidylcholine (DMPC) and dipalmitoylphosphatidylcholine (DPPC) as model lipid molecules [87,88]. Fig. 1 illustrates how we "built up" the lipid force field for saturated chain lipids using linear alkanes, dimethylphosphate, tetramethyl-ammonium, and methyl acetate as small molecule model compounds. While developing the small molecule analogs, we target properties including gas-phase electrostatic properties (dipole moments, atomic partial charges, molecular polarizabilities), gas-phase interaction energies and geometries of small molecule compounds with water (using the TIP4P-FQ model [3] as our solvent to which the force field is coupled), condensed phase bulk liquid properties for alkanes (densities, vaporization enthalphies, self-diffusion constants, relative torsional energetics), and

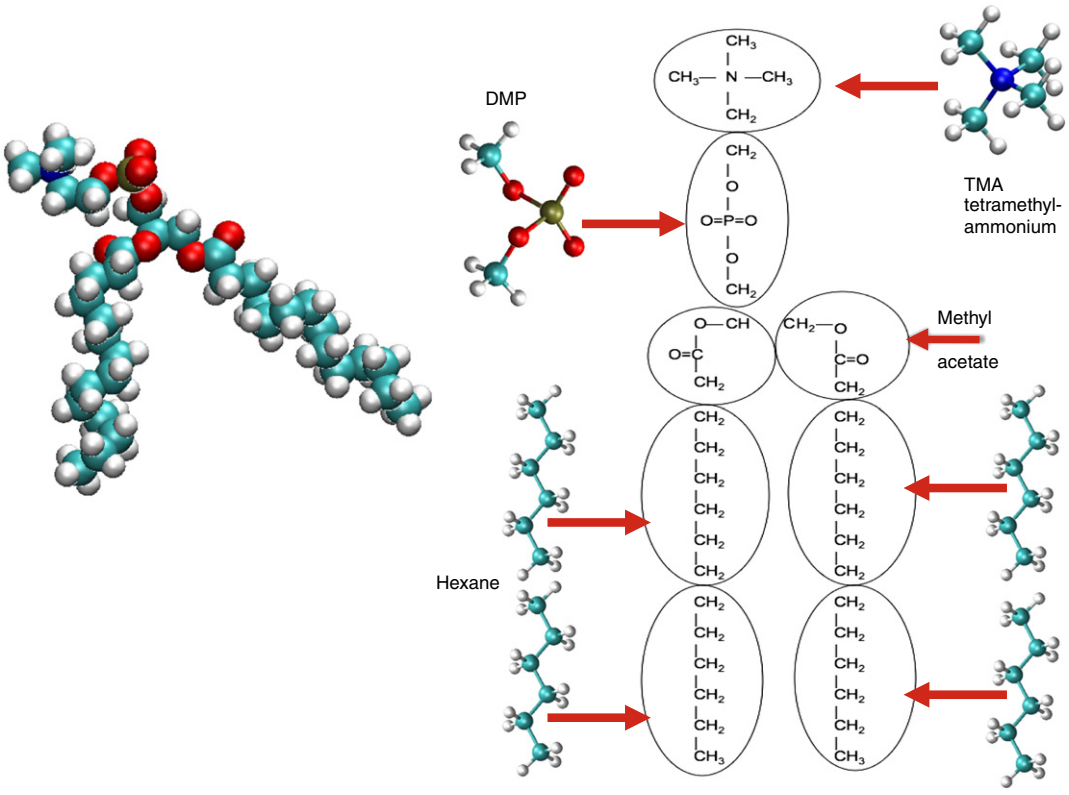

Fig. 1. Schematic of the partitioning of DMPC lipid molecule into small-molecule analogs for parameterization of the CHEQ lipid force field.

hydration free energies of linear alkanes in water [54]. Subsequent to the development of the DMPC/DPPC lipids in the CHEQ force field, the original CHEQ alkane force field [89] was refined using pair-specific Lennard–Jones interactions [90] in order to reduce the gain in free energy upon hydration predicted by the original force field; implications of this improvement influence the ability of water to permeate into the hydrophobic core of the bilayer as is discussed in the next section. A range of lipid bilayer properties were computed following the parameterization process. These include bilayer structure (electron density profile, atomic number density profiles), deuterium order parameters, phosphate–nitrogen (P–N) vector orientation, and dipole potential. The properties predicted using the CHEQ force field in general are as competitive as what were at the time counter-part fixed-charge force field. This set of properties is often taken as a first benchmark for development of force fields of a wide variety, be they all-atom, coarse-grained, or something in between the two extremes. As a first test, such properties are important to target in the force field development strategy.

3.1. Application of CHEQ lipid force fields

3.1.1. Influence of water polarization on free energetics of water permeation into bilayers

In our simulations of fully polarizable water/DMPC lipid bilayer systems, increased water permeation into the hydrophobic core of the bilayer occurs relative to the nonpolarizable CHARMM27 and CHARMM27R force fields [87]. This can be seen as an increased water number density beyond the carbonyl groups and reduced potential of mean force (PMF) for water entering the lipid tail region. The PMF calculated from water density profiles generated from long (40 ns), unbiased simulations of the solvated CHEQ DMPC bilayer suggest a 5 kcal/mol barrier for moving a water molecule from bulk to lipid interior [87], although subsequent analysis using more rigorous approaches such as the Weighted Histogram Analysis Method (WHAM) [91] suggest this barrier may as low as 4.5 kcal/mol [92]. The nature of water within the bilayer medium, with particular attention to how much would be present with the inclusion of integral membrane proteins, is an important consideration in the context of recent discussion about the energetics of charged species in low-dielectric bilayer media [76,93].

Ongoing efforts toward refinement of the interactions between small molecules with water continue to be of interest in the context of water permeation into the lipid bilayer interior. A recent study [90] presents refined interactions between small-chain alkanes and water, yielding alkane hydration free energies that are less favorable than those calculated using the original CHEQ force field [87]. For hexane, the reparameterization resulted in $\Delta G_{hydration} = 2.5 \pm 0.2$ kcal/mol (compared to the experimental value of $\Delta G_{hydration} = 2.550$ kcal/mol); this is approximately 0.7 ± 0.5 kcal/mol higher than the original parameterization [54]. When incorporated into the DMPC lipid bilayer model, the revised parameterization predicts a PMF barrier nearly 0.8 kcal/mol larger than the original parameterization. This is not surprising as an enhancement is expected from the less favorable interaction between water and the alkane. The range in values for the PMF barrier for different DMPC parameterizations (4.5–5.3 kcal/mol) is still generally lower than the values predicted from similar studies using nonpolarizable models (5.4–13 kcal/mol) [87,94–96].

3.1.2. Monolayer dipole potential

The membrane dipole potential plays an important role in the movement of molecular and ionic species across the water-lipid interface. A recent study using Drude oscillator models of the DPPC monolayer explored the surface dipole potential of a water-lipid monolayer system [97]. The authors demonstrated the improvement in the prediction of the relative interfacial potential, $\Delta V = V_{monolayer-air} - V_{water-air}$, over fixed-charge nonpolarizable force field representation. The authors suggest that, compared to the bilayer dipole potential, the monolayer potential is a less ambiguous measurement for comparing force

field predictions to experiment. We note that measurements of the bilayer dipole potential, values of which can be found in the literature for a wide spectrum of lipids using a variety of techniques including ion conductance, [98–100] cryo-EM, [64] and AFM, [101] are based on a number of approximations and are not a direct measure of the individual contributions to interfacial electrostatic properties arising from the presence of a lipid assembly. Ion conductance measurements, for instance, measure the permeability of a membrane to two structurally similar, oppositely charged hydrophobic ions tetraphenylborate (TPB^-) and tetraphenylarsonium (TPA^+) or tetraphenylphosphonium (TPP^+). The conductance measurements operate on the assumption that these ions, having the same interaction energies with hydrating water molecules, will have identical transfer free energies from water to any other medium and that a value for the membrane dipole potential can be calculated by extension. The validity of this assumption had been challenged using quantum mechanical calculations which found variations in the hydration energies of TPB^-, TPA^+, and TPP^+ [102]. Though quantum mechanical calculations with various treatments of solvent effects do show differences between the hydration properties of both ions, it is difficult to assess the magnitude of the difference with purely quantum methods which may or may not account for solvation effects. Schurhammer and coworkers have also explored the variation in hydration free energies for the TPB^-/TPA^+ system using molecular dynamics simulations and free energy perturbation calculations [103]. The authors find that TPB^- is more favorably hydrated than TPA^+, and that the difference in hydration free energy between the two is strongly dependent on the specific charge distribution; the range of differences in hydration energies is from 4.3 kcal/mol to 25 kcal/mol. Moreover, recent studies investigating the effects of charge asymmetry on hydration free energies of model asymmetric polar molecules by Mobley et al. [104] demonstrate significant differences in hydration free energies of oppositely polarized molecules, with these differences approaching the order of 10 kcal/mol. The notion of asymmetric hydration of small spherical ions as well as larger hydrophobic ions has been pursued extensively in the literature, though there still appears to be no consensus on the decisive relevance of the tetraphenylarsonium tetraphenylborate (TATB) assumption to the absolute bilayer dipole potential [105–110].

Acknowledging inherent ambiguities in the experimental determination of the membrane bilayer dipole potential, we, as the authors of the study in Ref. [97] consider the difference between the dipole potential of the water-monolayer and pure water liquid–vapor interfacial system.

The surface potential of a system can be calculated through double integration of charge density as a function of distance from the center of the water layer along the monolayer normal: [111]

$$V(z) = -\frac{1}{\epsilon_0}\int_{\infty}^{z}\int_{\infty}^{z'}\rho\left(z''\right)dz''dz'. \tag{13}$$

Here, ϵ_0 is the permittivity of vacuum and $\rho(z)$ is the charge density achieved by segmenting the system into slices of width dz and summing the atomic partial charges within each slice. This effectively solves the Poisson Equation assuming in-plane isotropy at a particular depth into the monolayer. For both of the interfacial systems the vacuum regions are referenced to a potential of 0 V and integration in Eq. (13) is taken from the vacuum region (∞) to a point at the center of the bulk water layer. To characterize the total membrane surface potential the charge densities of individual molecular species were twice integrated to yield constituent contributions to the electrostatic potential. Independently the surface potentials of these systems do not provide experimentally meaningful quantities but comparing the difference between the two,

$$\Delta V = V_{monolayer-air} - V_{water-air}, \tag{14}$$

yields the shift in the surface potential upon addition of a lipid monolayer onto the water–air interface. The monolayer dipole potential calculated in this way is an explicit property of the system and should provide insight into the electrostatic properties of lipid membranes. The results of this analysis for the total and constituent contributions to the surface potential of the monolayer system are shown graphically in Fig. 2, with the numerical values listed in Table 1. For comparison, Table 1 also includes surface potential values reported by Harder et al. (utilizing a fully polarizable Drude oscillator model) [97] as well as their results using the nonpolarizable CHARMM27 force field and the TIP3P water model. To investigate the effects of the variation of the water model on the potential calculation, the partial charges of the TIP4P-FQ water model used with the CHEQ force field were substituted with those of the nonpolarizable TIP3P water model in both the monolayer-air and water–air systems. The results of this analysis are also included in Table 1. Experimentally determined surface potential changes for phosphacholine lipids at the argon–water interface range from 0.30 to 0.45 V [112].

Fig. 2 shows the various contributions to the monolayer-air interfacial potential using the CHEQ model. The total interfacial potential for the monolayer-air system is 1.18 V; the pure water interfacial potential for the TIP4P-FQ water model is 0.54 V. The resulting difference in interfacial dipole potential is 0.64 ± 0.02 V, offering an improvement over the value of 0.8 V reported for the nonpolarizable CHARMM27 force field [97], though still overestimating this property relative to experiment. It is encouraging that the addition of explicit electronic polarization within a partial atomic charge formalism moves the prediction of monolayer potential closer to experiment relative to the fixed-charge force field. When the partial charges of TIP4P-FQ water are substituted with those of TIP3P, the membrane potential decreases to a value of 0.35 ± 0.02 V, matching the value reported for the Drude oscillator model and in close agreement with the experimental range. The change in the value of the dipole potential difference resulting from the artificial modification of water model charges at most suggests that the nature of the charge distributions and polarizability of the water model may be a first-order perturbation to consider when refining the combination of lipid and solvent force fields for molecular simulations of these types of biological systems.

We finally consider an ad hoc approach to consider the effect of polarization on the monolayer dipole potential. For this analysis, we use the trajectory snapshots generated from MD simulation using the fully polarizable CHEQ force field (water and lipids are fully polarizable). We then use gas-phase charges associated with a structurally

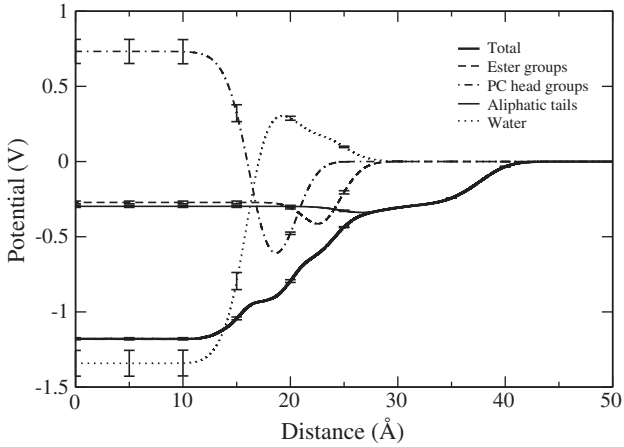

Fig. 2. Interfacial potential profiles of the total system and of selected components as a function of distance along the monolayer normal. The potential in the vacuum region is referenced to a value of 0 V.

Table 1
Component and total interfacial potential values (in Volts) of monolayer-air and water–air systems, including results reported for nonpolarizable (CHARMM27), polarizable Drude oscillator, and polarizable CHEQ force field. Results obtained using the CHEQ force field with TIP3P charge substitution are also shown.

	Drude [97]	CHARMM27 [97]	CHEQ	CHEQ/TIP3P
V_{water}	4.2	2.6	1.34	1.10
$V_{PC/head}$	−2.9	−2.4	−0.73	−0.73
V_{ester}	−0.1	0.7	0.27	0.27
$V_{aliphatic/tail}$	−0.3	0.4	0.30	0.30
$V_{monolayer-air}$	0.9	1.3	1.18	0.94
$V_{water-air}$	0.55	0.5	0.54	0.59
ΔV	0.35	0.8	0.64	0.35
$\Delta V_{Expt.}$		0.30–0.45		

minimized lipid (shown in Fig. 3) to compute the monolayer dipole potential. The differences in gas-phase charges for a single lipid in different conformations of the tails are observed to be neglible, so we continue the analysis with the charges associated with the structure shown in Fig. 3. We also strongly caution that the structures sampled using the fully polarizable force field may not include all of the relevant structures that would be sampled by MD simulations using the gas-phase charges. Thus, some care is warranted in the interpretation of the results of such ad hoc turning on and off of polarization effects. Fig. 4 shows the results of the monolayer-water dipole potential computed using the gas-phase minimized charges. From this analysis, we in fact observe a significant enhancement of the dipole potential when the effects of polarization are effectively switched off in this manner. Polarization, as observed in other studies, generates an opposing potential (field) that reduces the overall potential difference. The overall monolayer-water potential approaches −1.5 V (compared to −1.18 V for the fully polarizable system). Commensurate enhancement of the individual component contributions to the potential is also observed by comparison of Figs. 4 and 2.

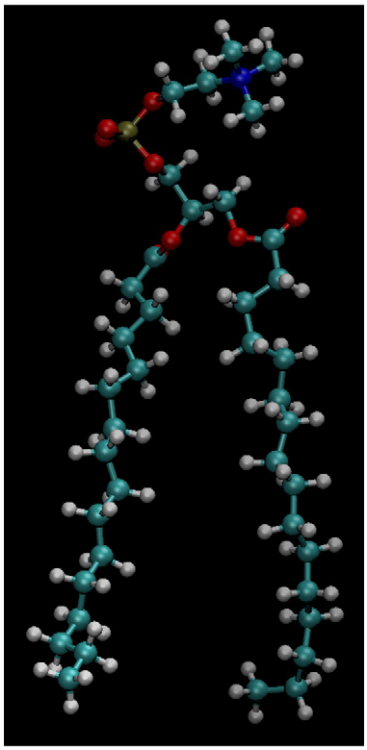

Fig. 3. Coordinate snapshot of a DPPC molecule extracted from the monolayer-water system and used for gas-phase charge minimization. Figure generated using Visual Molecular Dynamics [131].

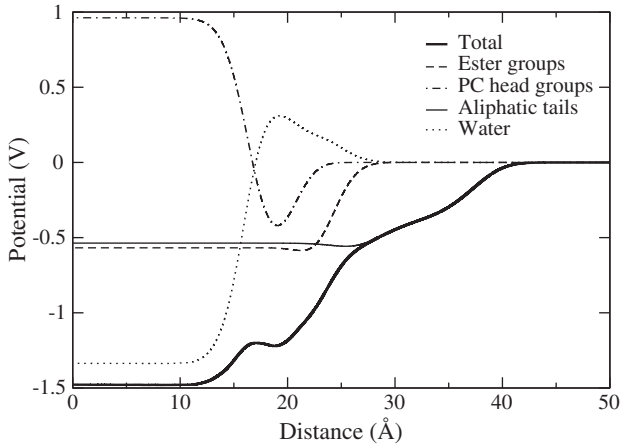

Fig. 4. Interfacial potential profiles of the total system and of selected components as a function of distance along the monolayer normal. Lipid atomic partial charges were substituted with those found from gas-phase charge minimization of a single DPPC molecule. The potential in the vacuum region is referenced to a value of 0 V.

3.2. Potassium ion permeation free energetics in gramicidin A

We used the charge equilibration polarizable force field for lipids, water, and protein to study the permeation free energy of potassium cation through the well-studied bacterial channel gramicidin A. The small, hard potassium cation is treated as a non-polarizable entity. This is a sufficiently justified approximation as the polarizability of potassium is 0.83 Å^3, [113] which is considerably smaller than the polarizability of solvent, lipid, and protein constituents. Moreover, without performing full hydration free energy calculations to gauge the ion–water and ion–protein interactions, we computed gas-phase interaction energies for K^+ with TIP4P-FQ (solvent model employed currently) and the N-Methylacetamide (NMA) molecule (as an often-used proxy for interactions with peptidic backbone). The current force field combination yields a TIP4P-FQ to ion interaction energy of −15.7 kcal/mol and an NMA to potassium ion interaction energy of −28.5 kcal/mol. The respective ab initio binding affinity values are −15.65 and −30.02 kcal/mol, respectively, based on the BSSE-corrected G2(MP2,SVP)ASC thermochemical approach from Ref. [114]. The binding affinity computed in this study effectively mimics the binding interaction energy at 0 K and affords an alternate set of values to compare the quality of the force field in lieu of costly solvation free energy calculations. The experimental binding affinity (enthalpy) values are −16.2 and −29.83 kcal/mol, respectively [114]. Thus the current force field captures the relative driving force for partitioning between bulk solvent and peptide channel (at least at the level of matching high-level gas-phase binding affinity measures in the form of experiment and ab initio calculations [114]). We note that the CHARMM27 force field predicts a K^+ to water binding energy of −18.9 kcal/mol and a K^+ to NMA binding energy of −24.20 kcal/mol. Thus, the original CHARMM27 non-polarizable force field underestimates the relative driving force for ion partitioning into the channel. The relative driving force ($\Delta\Delta E_{binding} = \Delta E_{K^+-NMA} - \Delta E_{K^+-H2O}$) is −5.3 kcal/mol for the CHARMM27 non-polarizable force field, −12.9 kcal/mol for the CHEQ force field, and −12.22 for the high-level ab initio values [20]. Structural integrity of the gA channel is monitored via the root-mean-squared deviation from the initial structure, obtained by equilibrating the crystal structure (PDB entry 1JNO); the RMSD remains well below 1 Å for the peptide in all windows [115]. Fig. 5 shows the one-dimensional potential of mean force computed using umbrella sampling with post-simulation data processing using the WHAM equations [91]. The uncorrected PMF shows a dramatic decrease in the central barrier to ion permeation, being almost one-

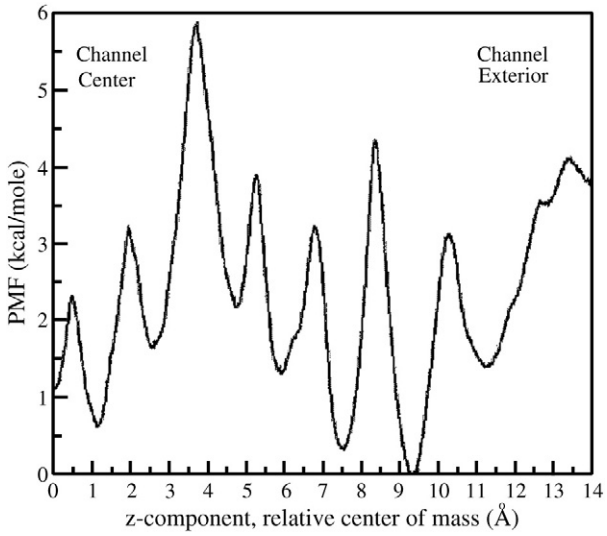

Fig. 5. Potential of mean force for potassium permeation in gramicidin A. Channel center is $z=0$. The x-axis corresponds to the z-component of the center of mass separation between the gA dimer and K^+ ion.

half to of the barrier predicted by standard forcefields. The global minimum occurs at 9.5 Å relative center of mass separation, in excellent agreement with the solid state ^{15}N NMR chemical shift anisotropy experiments of Tian et al. [116] as well as the ^{13}C NMR measurements of Smith and coworkers [117] for labeled gramicidin A analogs prepared in DMPC bilayers. Moreover, the site at 7.5 Å is seen to be of low free energy (almost commensurate in stability to the global binding site) but separated by a significant free energy barrier of 5 kcal/mol. This further coincides with the NMR measurements [116] suggesting an internal binding site of significantly reduced signal relative to the external binding sites (conjectured to be of equal free energetics).

3.3. The importance of charged species in membrane bilayer centers

Voltage-gated ion channels respond to transmembrane potential variations by opening and closing ion-conducting pores. The dynamics involved with this opening and closing are associated with conformational changes in the voltage sensor regions, locations where crystal structures suggest the presence of a series of charged arginine residues exposed to lipids. The notion of bare charged groups in bilayers is counter to the large hydration free energy of charged Arg (−60 kcal/mol) [76,118].

Previous experiments based on translocon experiments suggested barriers of helix-associated Arg translocation through the lipid environment on the order of 0.5 to 3 kcal/mol [93,119]. Previous MD studies using all-atom force fields and structurally well-defined model peptides with Arg side chains demonstrated the sequestering of Arg in the low-dielectric bilayer environment by 1.) water penetration into the bilayer and solvation shell formation around the Arg and 2.) deformation of the bilayer to allow zwitterionic headgroup interactions with the Arg [76,120]. We have recently shown, that using polarizable models for solvent and lipid gives rise to significantly different water penetration/permeation behavior into lipid bilayers [87,92]. Due to the ability of the water to change its electronic state (reflected in a shift of water dipole moment from the bulk value of 2.6 D to 1.9 D in the channel interior) polarizable water incurs less free energy penalty (based on estimated PMFs). In this scenario, one can imagine whether water alone would be sufficient to hydrate and effectively sequester polarizable side chains such as Arg within lipidic environments. If so, the rather large deformation of the lipid bilayer constituents would be lessened, though not necessarily obviated.

McCallum and Tieleman [65,121] presented umbrella sampling MD simulations of amino acid side chain analogs from water into DOPC, thus addressing the free energetics of side chains in lipidic environments. The authors also observed water defects, i.e., water molecules in the bilayer, providing a solvation layer for the translocating species. Furthermore, for the case of Arg, the calculations predicted that both the charged and uncharged forms are almost identically stable. The notion of water defects (and membrane deformation to some extent) is also invoked to explain the results. Of course, these calculations are performed with fixed-charge force fields. In the present study, we apply our charge equilibration force field in conjunction with umbrella sampling molecular dynamics simulations to consider the potential of mean force associated with methyl guanidinium (mguan) permeation from bulk solution to bilayer center; mguan serves as a small species analog for an arginine side chain. We present our model for the mguan interaction with solvent and lipid, the simulation methodology, and results of the total potential of mean force as well as the decomposition of the PMF into constituent contributions.

The charge equilibration, polarizable interaction model for methyl guanidinium was constructed starting with the CHARMM CHEQ force field for proteins developed by Patel and Brooks [47,48]. The electrostatic parameters, hardnesses and electronegativities, are transferred directly from the protein force field. The methyl guanidinium is partitioned into two charge normalization units to control polarizability scaling. The molecular polarizability of methyl guanidinium in this model is 6.41 $Å^3$ compared to the value of 7.02 $Å^3$ based on MP2/aug-cc-pVTZ calculations. The reduction from gas-phase prediction is consistent with the physical reduction in intrinsic molecular polarizability of molecules observed, in theory, using several methods; we note that the exact reduction in the condensed phase is certainly unknown, and this continues to pose a stubborn challenge for force field development in this area.

The existing non-bond (Lennard–Jones) interactions between methyl guanidinium and the headgroup and solvent entities were validated by comparison to high-level quantum mechanical energies as shown in Table 2. The correspondence with MP2/aug-cc-pVTZ optimized geometries and energies is rather good, particularly when considering the empirical adjustments that are usually necessary for quantitative reproduction of condensed-phase properties and the attendant loss of accuracy with respect to quantitative matching of ab initio reference data.

Table 2
Interaction energies between methyl guanidinium (mguan) and dimethylphosphate (DMP), tetramethylammonium (TMA), water (H_2O), or chloride ion (Cl^-) calculated using the CHEQ force field (FF) and ab initio (QM) calculations performed at the MP2/aug-cc-pVTZ level of theory. The range of values given for interactions with mguan with TMA represents the values obtained given variations in central distance between the two like charged species from 5.7 to 22.7 , while the ab initio interaction energy is for an analogous structure at a central atom separation of 6.1 . The three values given for interactions of mguan with either water or chloride represent three unique, stable geometries of the water or chloride around mguan.

Molecule	q (e)	E_{int}^{FF} (kcal/mol)	E_{int}^{QM} (kcal/mol)
Mguan	1	–	–
DMP	−1	−113.725	−120.331
TMA	1	58.669–14.464	51.940
H_2O	0	−12.824	−16.573
		−12.001	−16.419
		−11.795	−13.389
Cl^-	−1	−93.618	−114.547
		−92.190	−112.321
		−91.632	−115.634

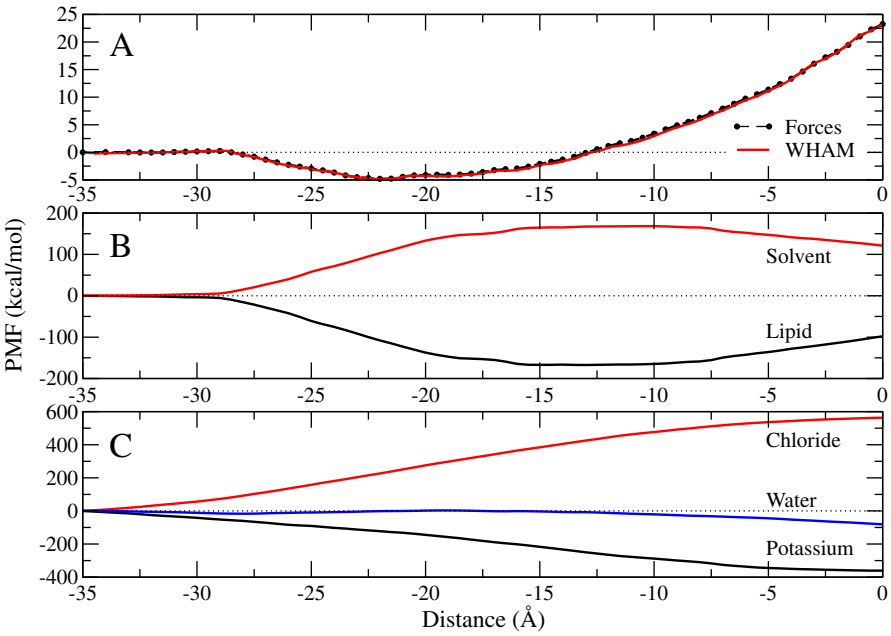

Fig. 6. Potential of mean force for moving a methyl guanidinium cation from bulk water to the center of a DDPC lipid bilayer. (a) Comparison of the PMF calculated using the Weighted Histogram Analysis Method [91] and directly from the forces acting on the cation. (b) Decomposition of the PMF into contributions from the DPPC bilayer (lipid) and the solvent (containing water, potassium, and chloride). (c) Decomposition of the solvent contribution to the PMF into water, chloride, and potassium contributions. In all panels, a horizontal dashed line is included as a visual guide to denote 0 kcal/mol.

3.4. Potential of mean force

We use umbrella sampling molecular dynamics simulations coupled with the Weighted Histogram Analysis Method [91] to sample the equilibrium potential of mean force along the reaction coordinate taken to be the center-of-mass difference (*z*-component) between the methyl guanidinium and bilayer centers of mass. We use the CHARMM miscellaneous mean field potential (MMFP) utility to impose the center of mass restraint. In addition, we impose a planar constraint on the center-of-mass of the lipid bilayer to prevent drift of the lipid in the *z*-direction and to maintain the system geometry. We begin with the free methyl guanidinium in solution to generate initial coordinate sets for the solute in bulk solution. We sample positions in solution using a harmonic umbrella position with force constants that vary along the reaction coordinate depending on the steepness of the underlying free energy surface. Using coordinates from one restraint window where the fluctuations allow the center of mass distance between mguan and bilayer center to take on the value for the next window, we start the restraint simulations in progressive windows to fill out the reaction coordinate. This is a standard protocol and the literature can be reviewed for further details of the procedure [75,93,115]. We monitor the overlap of the center of mass difference variable between windows to ensure sufficient overlap of distributions. Each window is sampled with between 5.0 and 7.5 ns of MD simulations which is sufficient to reach equilibrium. In addition, we use the definition of the potential of mean force as the interaction potential arising after integrating out all other degrees of freedom except the reaction coordinate of interest. This alternative is used to self-consistently check the umbrella sampling (WHAM based) potential of mean force, as well as to decompose the total potential of mean force into constituent contributions.

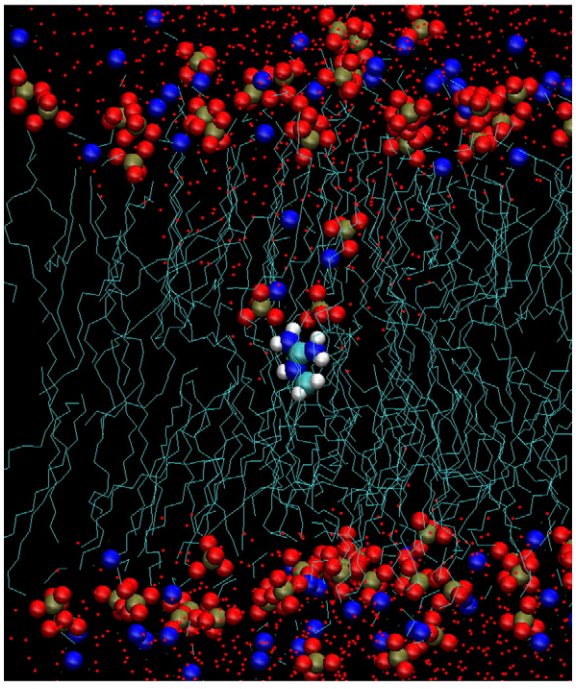

Fig. 7. Coordinate snapshot of methyl guanidinium in the center of the DPPC lipid bilayer visualized using Visual Molecular Dynamics [131].Water oxygen atoms are shown as red points and lipid carbon bonds are shown as light blue lines. Methyl guanidinium carbon (light blue), nitrogen (dark blue), and hydrogen (white) atoms are shown as well as lipid headgroup phosphorus (gold), nitrogen (dark blue), and oxygen (red) atoms.

Fig. 6 shows the total PMF for methyl guanidinium permeation from bulk to bilayer center using both the WHAM and force integration approaches. Both approaches give the same result, attesting to the self-consistency of the calculation. We observe a total barrier of about 28 kcal/mol relative to the global minimum occurring when the mguan experiences the strong local electrostatic fields in the region of the highly charge headgroups. This profile is not significantly different when compared to previously published results with non-polarizable force fields, though perhaps slightly more unfavorable by several kcal/mol [76,93]. The higher barrier may be a result of

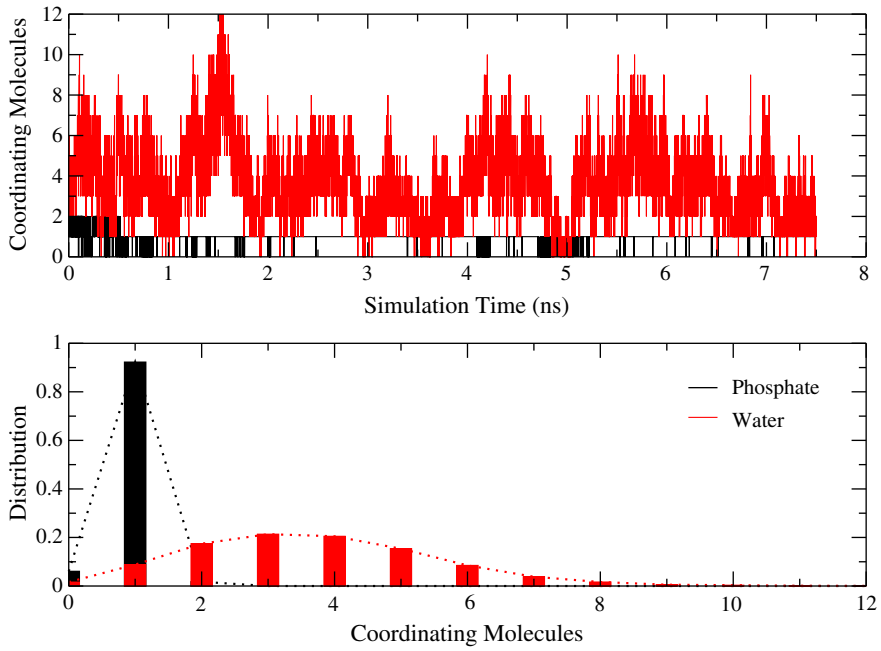

Fig. 8. Number of coordinating lipid phosphorus and water molecules (within 5 Å) around methyl guanidinium in the center of the DPPC lipid bilayer shown as a function of the simulation time (top) and the distribution over all data (bottom).

stronger mguan-headgroup interactions realized with the current CHEQ force field in relation to what is determined using non-polarizable models; furthermore, slight differences in the hydration free energetics of methyl guanidinium (water versus alkane-like environment) between the polarizable and fixed-charge force fields would also give rise to such differences in total barriers. Decomposing the total potential of mean force into contributions from water, total lipid (entire molecule), potassium ions, and chloride ions, we find that local-coordination with phosphate and water stabilizes the positively charged methyl guanidinium in the bilayer center. We observe in the restrained dynamics simulations that during the entire trajectories where the mguan is in the low-dielectric medium, there is, in 94% of the simulation snapshots, at least one strongly associating phosphate group pulled into the bilayer center (Fig. 8). This results in local deformation of the bilayer. Interestingly, the water also exerts a stabilizing effect; this comes from locally-coordinated water molecules (as observed during the MD trajectories). Intriguingly, the significant (and in our calculations, only) force destabilizing mguan in the bilayer center comes from the negatively-charged chloride ions in solution and intercalating in the headgroup region. In our simulations, this unfavorable contribution is up to 600 kcal/mol, with the positively-charged potassium ions contributing a major stabilizing interaction through a similar mechanism. Fig. 7 shows a snapshot from a trajectory in which mguan is constrained to be a normal distance of 0 Å from the bilayer center of mass. We observe that the water and phosphate coordination is quite local. Fig. 8 shows time profiles and distribution of the number of water molecules and phosphates (from lipid headgroups) coordinating (within 5 Å) with the buried arginine side chain. This again confirms the importance of the core waters and headgroups in stabilizing the mguan in this scenario from the large destabilizing effects of the anions.

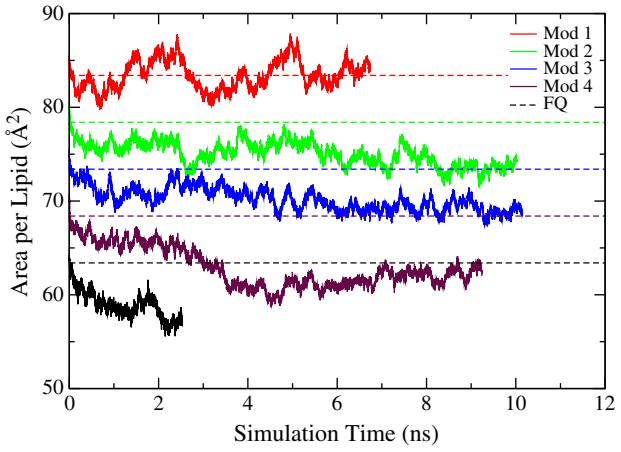

Fig. 9. Area per lipid as a function of time for different parameter set modifications as well as the unmodified (FQ) force field. The profiles are offset by 5 for clarity and horizontal dashed lines correspond to the experimental area per lipid value of 63.4 Å^2.

3.5. Future directions

Having established and successfully applied a first-generation polarizable force field for lipid bilayers and integral membrane proteins and peptides, we propose to continue the development of the force field for an extended palette of lipid molecules as well as to refine the current model for phosphacholine (PC) lipids with respect to the surface area per lipid head group and deuterium order parameter, S_{CD}, profiles. Fig. 9 shows time profiles of the surface are per lipid from multiple *NPT* molecular dynamics simulations (no external surface tension applied to the unit cell) of a solvated DPPC bilayer. The first generation force field predicts a non-zero surface tension (with the accepted surface tension of bilayers being zero) which results in a surface area per lipid molecule being too small (Surface Area(simulation) = 57 Å^2/lipid, Surface Area(experiment) = 63.4 Å^2/lipid). To improve agreement with experimental values, we will tune interactions between headgroups to match ab initio quantum mechanical data since there is no direct experimental measurement of such interactions. This is a novel and systematic approach compared to previous attempts to modify/refine existing non-polarizable force fields.

Since the lipid-water interfacial area obtained using the original CHEQ lipid force field in conjunction with the TIP4P-FQ water model is effectively smaller than experiment (Fig. 9), we computed interaction energies and structures of model compounds representing the head

Table 3
Non-bond parameters, geometric separation, and interaction energy between DMP and TMA. R_{P-N} denotes the separation distance between the two molecules measured between the phosphorus of DMP and the nitrogen of TMA. FQ denotes the original CHEQ force field parameters and interactions.

O2L-NTL Mod	ϵ (kcal/mol)	R_{min} (Å)	R_{P-N} (Å)	$E_{interaction}$ (kcal/mol)
MP2/631++g(2d,p)	–	–	4.17	−95.4934
FQ	−0.114	3.78	4.02803	−102.3194
1	−0.114	4.80	4.20456	−97.2246
2	−0.114	4.75	4.18488	−97.7777
3	−0.114	4.70	4.16802	−98.2965
4	−0.114	4.60	4.13874	−99.2225

group moieties, namely dimethylphosphate and tetramethylammonium ions. Optimized geometries for various complexes were computed at the MP2/631++g(2d,p) level of theory. Table 3 summarizes the calculations. We observe that we can systematically modulate the inter-headgroup interactions by modifying the Lennard–Jones interactions using pair-specific interaction parameters to model the off-diagonal interaction parameters. This approach has been applied previously in our and other laboratories [90].

We will continue refinement of deuterium order parameter profiles (S_{CD}) by revisiting torsional energy profiles as has been successfully implemented for the development of the CHARMM C36 lipid force field ([85]). Using similar model compounds to mimic the relative torsions, we will fit dihedral parameters for the CHARMM torsional function as we have done in the past. Preliminary data from results of fitting are shown in Fig. 10.

4. Conclusions and discussion

With the continuing advances in computational hardware [122,123] and novel force fields constructed using quantum mechanics, the outlook for non-additive force fields is promising. Our work in the past several years has slowly demonstrated the utility of polarizable force fields, particularly those based on the charge equilibration formalism, for a broad range of physical and biophysical systems. We have constructed polarizable force fields for small molecules [47,53–55,124–126], proteins [48], lipids, and lipid bilayers [87,115,127,54,128].

Our methodology for parameterizing charge equilibration force fields has proven successful as we have been able to derive a first-generation polarizable force field for lipid bilayers that is fully and self-consistently polarizable. The force field is coupled with the TIP4P-FQ charge equilibration water force field, though with care, one may apply the lipid force field with other water models, both polarizable (such as the Drude oscillator model) or fixed-charge models. We have validated the force field against a number of properties classically considered in the context of development of all-atom and coarse-grained models for lipids and bilayers; these include structure (electron and atom density profiles), deuterium order parameter profiles, membrane and monolayer dipole potentials, P–N angle vector distributions, and others [54,87].

We have successfully applied our models for long molecular dynamics simulations to practical applications. We have considered the difficult test case of the gramicidin A bacterial channel, long-held to be a rigorous test case for all-atom force fields [115]. Our first-generation force field in conjunction with the water and protein force field based on the charge equilibration formalism predicted an equilibrium potential of mean force that was significantly different than that predicted by nonpolarizable models. Under similar assumptions as previous studies, we estimate that the predicted single-channel conductance is higher and closer to experiment compared to previous predictions using fixed-charge models. Furthermore, this overall increase is related to the local electrostatic response of channel waters and pore-lining carbonyl oxygen atoms [115].

Our recent work exploring the free energetics of charged amino acid side-chain analogs translocating from bulk solution to bilayer center has provided intriguing results. Using the combination of interaction models discussed above, with all components polarizable except for the small, hard cations (potassium) and chloride anions (regarded as having marginal effects arising from specific ion polarizability in relation to the bromide and iodide, for instance), we find that the total potential of mean force reflects earlier results using both polarizable and non-polarizable force fields. However, our decomposition analysis suggests that the repulsive barrier for methyl guanidinium permeation arises from the attractive electrostatic field of the chloride ions in solution, while the locally-associated water (on average 1–6) and headgroup phosphate (on average 1) moieties stabilize the charged species. We anticipate that under more physiologically relevant salt

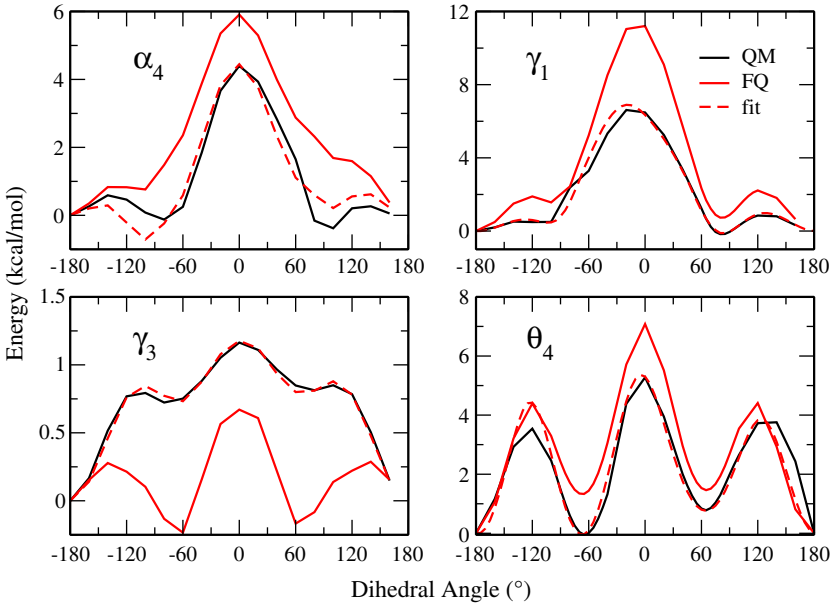

Fig. 10. Torsion profiles based on model compounds including propylmethylphosphate (PMP) and an esterified glycerol analog ((M)EGLY) and fit to ab initio data used in the most recent parameterization of the CHARMM nonpolarizable lipid force field [85].

concentrations, the barrier may be significantly reduced, or vanish, thus presenting an alternate view relating membrane deformation and bilayer water content to the stability of charged and polar groups in lipidic environments.

We finally note that charge transfer effects have largely been neglected in classical formalisms; the implications of charge transfer are now becoming more apparent for ion channels and condensed phase [14,60,129], and the development of interaction potentials capable of explicitly and dynamically including such effects is warranted, particularly for biophysical systems involving charge-dense ions [60].

With respect to biomacromolecular force fields, we have successfully constructed models for lipid molecules that we are now exploiting for molecular dynamics simulations of ion channels [115] and issues related to charge species in low-dielectric membrane environments [76,93,130]. Further development and refinement of such models continue aggressively in our lab.

Acknowledgements

The authors gratefully acknowledge the National Institutes of Health (NCRR) for their financial support (P20-RR017716, Chemistry and Biochemistry) and computational infrastructure (P20-RR015588, Chemical Engineering). We also thank Professor Jeff Klauda for providing the ab initio data in Fig. 10.

References

[1] I. Leontyev, A. Stuchebrukhov, PCCP 13 (2011) 2613–2626.
[2] W.C. Swope, H.W. Horn, J.E. Rice, Chem. Phys. Lett. 114 (2010) 8621–8630.
[3] S.W. Rick, S.J. Stuart, B.J. Berne, J. Chem. Phys. 101 (1994) 6141–6156.
[4] L.R. Olano, S.W. Rick, J. Comput. Chem. 26 (2005) 699–707.
[5] S.W. Rick, S.J. Stuart, J.S. Bader, B.J. Berne, J. Mol. Liq. 65/66 (1995) 31.
[6] A.K. Rappe, W.A. Goddard, J. Phys. Chem. 95 (1991) 3358–3363.
[7] P. Ren, J.W. Ponder, J. Comput. Chem. 23 (2002) 1497–1506.
[8] P. Ren, J.W. Ponder, J. Phys. Chem. B 107 (2003) 5933–5947.
[9] P. Ren, J.W. Ponder, J. Comput. Chem. 23 (2002) 1497–1506.
[10] M.A. Brown, R. D'Auria, L.F.W. Kuo, M.J. Krisch, D.E. Starr, H. Bluhm, D.J. Tobias, J.C. Hemminger, Phys. Chem. Chem. Phys. 10 (2008) 4778–4784.
[11] P. Jungwirth, D.J. Tobias, J. Phys. Chem. B 105 (2001) 10468–10472.
[12] P. Jungwirth, D.J. Tobias, J. Phys. Chem. B 106 (2002) 6361–6373.
[13] P. Jungwirth, D.J. Tobias, Chem. Rev. 106 (2006) 1259–1281.
[14] D. Bucher, S. Raugei, L. Guidoni, M. DalPeraro, U. Rothlisberger, P. Carloni, M.L. Klein, Biophys. Chem. 124 (2006) 292–301.
[15] M. Sprik, J. Chem. Phys. 95 (1991) 6762–6769.
[16] B. de Courcy, J. Piquemal, C. Garbay, N. Gresh, J. Am. Chem. Soc. 132 (2010) 3312–3320.
[17] J.-P. Piquemal, H. Chevreau, N. Gresh, J. Chem. Theory Comput. 3 (2007) 824–837.
[18] J. Applequist, J.R. Carl, K. Fung, J. Am. Chem. Soc. 94 (1972) 2952–2960.
[19] J.W. Caldwell, P.A. Kollman, J. Phys. Chem. 99 (1995) 6208–6219.
[20] A. Grossfield, P. Ren, J.W. Ponder, J. Am. Chem. Soc. 125 (2003) 15671–15682.
[21] A. Grossfield, J. Chem. Phys. 122 (2005) 024506.
[22] D. Jiao, C. King, A. Grossfield, T.A. Darden, P. Ren, J. Phys. Chem. B 110 (2006) 18553–18559.
[23] J.W. Ponder, C. Wu, P. Ren, V.S. Pande, J.D. Chodera, M.J. Schnieders, I. Haque, D.L. Mobley, D.S. Lambrecht, R.A. DiStasio Jr., M. Head-Gordon, G.N.I. Clark, M.E. Johnson, T. Head-Gordon, J. Phys. Chem. B 114 (2010) 2549–2564.
[24] P. Ren, J.W. Ponder, J. Phys. Chem. B 108 (2004) 13427–13437.
[25] B.T. Thole, Chem. Phys. 59 (1981) 341–350.
[26] V.M. Anisimov, G. Lamoureux, I.V. Vorobyov, N. Huang, B. Roux, A.D. MacKerell Jr., J. Chem. Theory Comput. 1 (2005) 153–168.
[27] G. Lamoureux, B. Roux, J. Chem. Phys. 119 (2003) 3025.
[28] G. Lamoureux, A.D. MacKerell Jr., B. Roux, J. Chem. Phys. 119 (2003) 5185.
[29] G. Lamoureux, E. Harder, I.V. Vorobyov, B. Roux, A.D. MacKerell Jr., Chem. Phys. Lett. 418 (2006) 245–249.
[30] P.E.M. Lopes, G. Lamoureux, B. Roux, A.D. MacKerell Jr., J. Phys. Chem. B 111 (2007) 2873–2885.
[31] I.V. Vorobyov, V.M. Anisimov, A.D. MacKerell Jr., J. Phys. Chem. B 109 (2005) 18988–18999.
[32] I.V. Vorobyov, V.M. Anisimov, S. Greene, R.M. Venable, A. Moser, R.W. Pastor, A.D. MacKerell Jr., J. Chem. Theory Comput. 3 (2007) 1120–1133.
[33] C.M. Baker, P.E.M. Lopes, X. Zhu, B. Roux, A.D. MacKerell Jr., J. Chem. Theory Comput. 6 (2010) 1181–1198.
[34] G. Lamoureux, B. Roux, J. Phys. Chem. B 110 (2006) 3308–3322.
[35] H. Yu, T.W. Whitfield, E. Harder, G. Lamoureux, I. Vorobyov, V.M. Anisimov, A.D. MacKerell Jr., B. Roux, J. Chem. Theory Comput. 6 (2010) 774–786.
[36] B. de Courcy, J.-P. Piquemal, C. Garbay, N. Gresh, J. Am. Chem. Soc. 132 (2010) 3312.
[37] M. Devereux, M.-C. van Severen, O. Parisel, J.-P. Piquemal, N. Gresh, J. Chem. Theory Comput. 7 (2011) 138–147.
[38] Chaudret, R.; Gresh, N.; Parisel, O.; Darden, T. A.; Cisneros, G. A.; Piquemal, J.-P. J. Chem. Phys. 2011, in revision.
[39] J.-P. Piquemal, B. Williams-Hubbard, N. Fey, R.J. Deeth, N. Gresh, C. giessner Prettre, J. Comput. Chem. 2003 (1963) 24.
[40] N. Gresh, J.-P. Piquemal, M. Krauss, J. Comput. Chem. 26 (2005) 1113.
[41] J.-P. Piquemal, G.A. Cisneros, P. Reinhardt, N. Gresh, T.A. Darden, J. Chem. Phys. 124 (2006) 104101.
[42] R.T. Sanderson, Science 114 (1951) 670–672.
[43] R.T. Sanderson, Chemical Bonds and Bond Energy, Academic Press, New York, 1976.
[44] S.W. Rick, B.J. Berne, J. Am. Chem. Soc. 118 (1996) 672–679.
[45] S.W. Rick, S.J. Stewart, Reviews of Computational Chemistry, John Wiley & Sons, New York, 2002.
[46] S.W. Rick, J. Chem. Phys. 114 (2001) 2276–2283.
[47] S. Patel, C.L. Brooks III, J. Comput. Chem. 25 (2004) 1–15.
[48] S. Patel, A.D. MacKerell Jr., C.L. Brooks III, J. Comput. Chem. 25 (2004) 1504–1514.
[49] S. Patel, C.L. Brooks III, J. Chem. Phys. 122 (2005) 024508.
[50] S. Patel, C.L. Brooks III, Mol. Simul. 32 (2006) 231–249.
[51] L.R. Olano, S.W. Rick, J. Comput. Chem. 26 (2005) 699–707.
[52] G.L. Warren, J.E. Davis, S. Patel, J. Chem. Phys. 128 (2008) 144110.
[53] Y. Zhong, G.L. Warren, S. Patel, J. Comput. Chem. 29 (2007) 1142–1152.
[54] J.E. Davis, G.L. Warren, S. Patel, J. Phys. Chem. B 112 (2008) 8298–8310.
[55] B.A. Bauer, S. Patel, J. Mol. Liq. 142 (2008) 32–40.
[56] C.J. Illingworth, C. Domene, Proc. R. Soc. A 465 (2009) 1701–1716.
[57] J.-P. Piquemal, L. Perera, G.A. Cisneros, P. Ren, L.G. Pedersen, T.A. Darden, J. Chem. Phys. 125 (2006) 054511.
[58] B.A. Bauer, G.L. Warren, S. Patel, J. Chem. Theory Comput. 5 (2009) 359–373.
[59] R.F. Nalewajski, J. Korchowiec, Z. Zhou, Int. J. Quant. Chem. 22 (1988) 349–366.
[60] A.J. Lee, S.W. Rick, J. Chem. Phys. 134 (2011) 184507.
[61] R. Chelli, P. Procacci, R. Righini, S. Califano, J. Chem. Phys. 111 (1999) 8569–8575.
[62] R. Car, M. Parrinello, Phys. Rev. Lett. 55 (1985) 2471–2474.
[63] H.A. Stern, S.E. Feller, J. Chem. Phys. 118 (2003) 3401–3412.
[64] L. Wang, P.S. Bose, F.J. Sigworth, PNAS 103 (2006) 18528–18533.
[65] J.L. MacCallum, W.F.D. Bennett, D.P. Tieleman, Biophys. J. 94 (2008) 3393–3404.
[66] N. Kučerka, Y. Liu, N. Chu, H.I. Petrache, S. Tristram-Nagle, J.F. Nagle, Biophys. J. 88 (2005) 2626–2637.
[67] N. Kučerka, J.F. Nagle, J.N. Sachs, S.E. Feller, J. Pencer, A. Jackson, J. Katsaras, Biophys. J. 95 (2008) 2356–2367.
[68] H.I. Petrache, S.W. Dodd, M.F. Brown, Biophys. J. 79 (2000) 3172–3192.
[69] D. Marsh, Eur. Biophys. J. 31 (2002) 559–562.
[70] D.A. Erilov, R. Bartucci, R. Guzzi, A.A. Shubin, A.G. Maryasov, D. Marsh, S.A. Dzuba, L. Sportelli, J. Phys. Chem. B 109 (2005) 12003–12013.
[71] J.C. Mathai, S. Tristram-Nagle, J.F. Nagle, M.L. Zeidel, J. Gen. Physiol. 131 (2008) 69–76.
[72] B. Roux, T. Allen, S. Berneche, W. Im, Q. Rev. Biophys. 37 (2004) 15–103.
[73] T.W. Allen, T. Bastug, S. Kuyucak, S.-H. Chung, Biophys. J. 84 (2003) 2159–2168.
[74] S. Berneche, B. Roux, Biophys. J. 82 (2002) 772–780.
[75] T.W. Allen, O.S. Andersen, B. Roux, PNAS 101 (2004) 117–122.
[76] S. Dorairaj, T.W. Allen, PNAS 104 (2007) 4943–4948.
[77] M.P. Aliste, D.P. Tieleman, BMC Biochem. 6 (2005) 30.
[78] D.P. Tieleman, J.L. MacCallum, W.L. Ash, C. Kandt, Z. Xu, L.M. Monticelli, J. Phys. Condens. Matter 18 (2006) S1221–S1234.
[79] Z. Xu, H.H. Luo, D.P. Tieleman, J. Comput. Chem. 28 (2007) 689–697.
[80] S.E. Feller, Curr. Opin. Colloid Interface Sci. 5 (2000) 217–223.
[81] J.L. MacCallum, D.P. Tieleman, J. Am. Chem. Soc. 128 (2006) 125–130.
[82] S.A. Pandit, D. Bostick, M.L. Berkowitz, Biophys. J. 86 (2004) 1345–1356.
[83] M.L. Berkowitz, D.L. Bostick, S.A. Pandit, Chem. Rev. 106 (2006) 1527–1539.
[84] S.W.I. Siu, R. Vacha, P. Jungwirth, R.A. Bockmann, J. Chem. Phys. 128 (2008) 125103.
[85] J.B. Klauda, R.M. Venable, J.A. Freites, J.W. O'Connor, D.J. Tobias, C. Mondragon-Ramirez, I. Vorobyov, A.D. MacKerrel Jr., R.W. Pastor, J. Phys. Chem. B 114 (2010) 7830–7843.
[86] R.W. Pastor, A.D. MacKerell Jr., J. Phys. Chem. Lett. 2 (2011) 1526–1532.
[87] J.E. Davis, O. Rahaman, S. Patel, Biophys. J. 96 (2009) 385–402.
[88] J.E. Davis, S. Patel, J. Phys. Chem. B 113 (2009) 9183–9196.
[89] S. Patel, C.L. Brooks III, J. Chem. Phys. 124 (2006) 204706.
[90] J.E. Davis, S. Patel, Chem. Phys. Lett. 484 (2010) 173–176.
[91] S. Kumar, D. Bouzida, R.H. Swendsen, P.A. Kollman, J.M. Rosenberg, J. Comput. Chem. 13 (1992) 1011–1021.
[92] B.A. Bauer, T.R. Lucas, D. Meninger, S. Patel, Chem. Phys. Lett. 508 (2011) 289–294.
[93] E.V. Schow, J.A. Freites, P. Cheng, A. Bernsel, G. von Heijne, S.H. White, D.J. Tobias, J. Membr. Biol. 239 (2011) 35–48.
[94] M. Orsi, W.E. Sanderson, J.W. Essex, J. Phys. Chem. B 2009 (2009) 12019–12029.
[95] T. Sugii, S. Takagi, Y. Matsumoto, J. Chem. Phys. 123 (2005) 184714.
[96] P. Jedlovszky, M. Mezei, J. Am. Chem. Soc. 122 (2000) 5125–5131.
[97] E. Harder, A.D. MacKerell Jr., B. Roux, J. Am. Chem. Soc. 131 (2009) 2760–2761.
[98] H. Brockman, Chem. Phys. Lipids 73 (1994) 57–79.
[99] R.J. Clarke, Adv. Colloid Interface Sci. 89 (2001) 263–281.
[100] K. Gawrisch, D. Ruston, J. Zimmerberg, V.A. Parsegian, R.P. Rand, N. Fuller, Biophys. J. 61 (1992) 1213–1223.

[101] Y. Yang, K.M. Mayer, N.S. Wickremasinghe, J.H. Hafner, Biophys. J. 95 (2008) 5193–5199.
[102] J. Schamberger, R.J. Clarke, Biophys. J. 82 (2002) 3081–3088.
[103] R. Schurhammer, E. Engler, G. Wipff, J. Phys. Chem. B 105 (2001) 10700–10708.
[104] D.L. Mobley, A.E. Barber, C.J. Fennell, K. Dill, J. Phys. Chem. B 112 (2008) 2405–2414.
[105] Y. Shao, A.A. Stewart, H.H. Girault, J. Chem. Soc., Faraday Trans. 87 (1991) 2593–2597.
[106] R. Schurhammer, G. Wipff, J. Phys. Chem. A 104 (2000) 11159–11168.
[107] V. Luzhkov, A. Warshel, J. Comput. Chem. 13 (1992) 199–213.
[108] B. Roux, H.-A. Yu, M. Karplus, J. Phys. Chem. 94 (1990) 4684–4688.
[109] G. Hummer, L.R. Pratt, A.E. Garcia, J. Phys. Chem. 100 (1996) 1206–1215.
[110] R.M. Lynden-Bell, J.C. Rasaiah, J. Chem. Phys. 107 (1997) 1981–1991.
[111] E. Harder, B. Roux, J. Chem. Phys. 129 (2008) 234706.
[112] J.M. Smaby, H.L. Brockman, Biophys. J. 58 (1990) 195–204.
[113] G. Mahan, Phys. Rev. A 22 (1980) 1780–1785.
[114] F.M. Siu, N.L. Ma, C.W. Tsang, J. Chem. Phys. 114 (2001) 7045–7051.
[115] S. Patel, J.E. Davis, B.A. Bauer, J. Am. Chem. Soc. 131 (2009) 13890–13891.
[116] F. Tian, T.A. Cross, J. Mol. Biol. 285 (1999) 1993–2003.
[117] R. Smith, D.E. Thomas, A.R. Atkins, F. Separovic, B.A. Cornell, Biochim. Biophys. Acta (BBA): Biomembr. 1026 (1990) 161–166.
[118] Y. Deng, B. Roux, J. Phys. Chem. B 108 (2004) 16567–16576.
[119] T. Hessa, S.H. White, G. von Heijne, Science 307 (2005) 1427.
[120] J.A. Freites, D.J. Tobias, G. von Heijne, S.H. White, PNAS 102 (2005) 15050–15064.
[121] J.L. MacCallum, W.F.D. Bennett, D.P. Tieleman, J. Gen. Physiol. 129 (2007) 371–377.
[122] B.A. Bauer, J.E. Davis, M. Taufer, S. Patel, J. Comput. Chem. 32 (2011) 375–385.
[123] Ganesan, N.; Bauer, B. A.; Lucas, T. R.; Patel, S.; Taufer, M. J. Comput. Chem. 2011, Submitted for publication, in revision.
[124] Y. Zhong, S. Patel, J. Phys. Chem. B 113 (2009) 767–778.
[125] Zhong, Y.; Bauer, B. A.; Patel, S. J. Comput. Chem. 2011, in revision.
[126] Y. Zhong, S. Patel, J. Phys. Chem. B 114 (2010) 11076–11092.
[127] S. Patel, Y. Zhong, B.A. Bauer, J.E. Davis, J. Phys. Chem. B 113 (2009) 9241–9254.
[128] Lucas, T. R.; Bauer, B. A.; Patel, S. J. Comput. Chem. 2011, in revision.
[129] Z. Zhao, D.M. Rogers, T.L. Beck, J. Chem. Phys. 132 (2010) 014502.
[130] I. Vorobyov, T.W. Allen, J. Chem. Phys. 132 (2010) 185101.
[131] W. Humphrey, A. Dalke, K. Schulten, J. Mol. Graph. 14 (1996) 33–38.